Journal of Materials Chemistry A

Thermally Induced Migration of a Polyoxometalate within a Metal–Organic Framework and its Catalytic Effects

Journal:	*Journal of Materials Chemistry A*
Manuscript ID	TA-COM-03-2018-002562.R1
Article Type:	Communication
Date Submitted by the Author:	08-Apr-2018

Complete List of Authors:	Buru, Cassandra; Northwestern University, Chemistry Platero-Prats, Ana; Argonne National Laboratory, X-ray Science Division Chica, Daniel; Northwestern University, Chemistry Kanatzidis, Mercouri; Northwestern University, Department of Chemistry Chapman, Karena; Argonne National Laboratory, X-ray Science Division Farha, Omar; Northwestern University, Department of Chemistry

Journal Name

COMMUNICATION

Thermally Induced Migration of a Polyoxometalate within a Metal–Organic Framework and its Catalytic Effects

Received 00th January 20xx,
Accepted 00th January 20xx

DOI: 10.1039/x0xx00000x

www.rsc.org/

Cassandra T. Buru,[a] Ana. E Platero-Prats,[b†] Daniel G. Chica,[a] Mercouri G. Kanatzidis,[a] Karena W. Chapman,[b] Omar K. Farha[a,c*]

The polyoxometalate (POM), $H_3PW_{12}O_{40}$, was postsynthetically incorporated into the metal-organic framework (MOF), NU-1000. The POM@MOF composite, PW_{12}@NU-1000, was activated under mild conditions, resulting in a material whose diffraction pattern and spectroscopic properties differ from the same material heated at elevated temperatures. These discrepancies, corroborated by difference envelope density analyses, were attributed to the POM residing either in the mesoporous or microporous channels of NU-1000. As a testament to the importance of catalyst accessibility, the POM's locational change also induced a change in the composite's rate and selectivity toward oxidizing 2-chloroethyl ethyl sulfide.

Active catalysts, ranging from single atoms[1] to molecular complexes[2] to large nanoparticles,[3] are often immobilized on heterogeneous supports in order to improve their reactivity by preventing aggregation and subsequent deactivation, while concurrently facilitating their separation from substrate and product allowing for reuse of the catalyst material.[4–6] Deposition on these supports is most commonly accomplished using electrostatic interactions, encapsulation, adsorption, precipitation, or covalent tethering.[7–9] Dependent on the nature of the support and catalyst, deposited species can adopt several positions and orientations. Precise knowledge and control over the three dimensional location of these active species on/in a support is essential for understanding the role of the support, as location can control reactivity and selectivity in some systems.[10–12]

Often sensitive to its environment and plagued with low surface area, polyoxometalates (POMs) are one such class of catalyst species that greatly benefit from being dispersion on solid supports.[13–15] POMs are highly soluble anionic metal oxide clusters composed of group V or VI transition metals, which can be partially substituted with virtually any element from the periodic table.[16–19] Their ability to undergo multielectron redox transformations allows for applications in redox catalysis.[20] Solid supports, including activated carbon,[21,22] mesoporous silica,[23,24] metal/metal oxide surfaces,[25,26] covalent-organic frameworks,[27] zeolites,[28] and metal-organic frameworks (MOFs),[29,30] have been used to stabilize POMs under catalytic conditions. The latter four benefit from crystalline structures, thereby permitting rapid structure determination of the POM/support composite. MOFs, composed of metal ion or metal oxide nodes connected by organic linkers,[31,32] are exceptional support materials as their tunability gives rise to several desirable properties, such as crystallinity, permanent porosity, high surface area, large apertures, and high chemical and thermal stability.[33]

Targeted assembling strategies toward POM/MOF composites often use a "bottle around ship" approach[34–36] or ion exchange[37,38] to direct a catalyst to a desired location; however, these systems lack the ability to further modify the POM's location postsynthetically. For example, MIL-101 has a hierarchical pore structure containing 29 Å and 34 Å pores connected via 12 Å or 16 × 15 Å apertures.[39] When Keggin-type POMs are incorporated into MIL-101 via impregnation, POMs are located in the larger mesopore only. On the other hand, when POM@MIL-101 is synthesized via encapsulation, the POMs are directed not only to the larger pores, but also to the smaller pores, which have apertures small enough to prevent the POM from leaching. The location of the POMs was found to have slight effects on the rates of reactions like acetaldehyde-phenol condensation and the acetalization of benzaldehyde.[40,41]

[a] Department of Chemistry, Northwestern University, 2145 Sheridan Road, Evanston, Illinois 60208, United States
[b] X-ray Science Division, Advanced Photon Source, Argonne National Laboratory, Argonne, Illinois 60439-4858, United States
[c] Department of Chemistry, Faculty of Science, King Abdulaziz University, Jeddah 21589, Saudi Arabia
† Current address: Department of Inorganic Chemistry, Universidad Autónoma de Madrid, 28049 Madrid, Spain.
*Email - o-farha@northwestern.edu

Electronic Supplementary Information (ESI) available: [materials, methods and instrumentation, synthesis details, SEM-EDS, in situ PXRD, DED, TGA, DSC, NMR, CV, total DRUV-vis, catalytic procedure, selectivity, 1 mol% reaction profiles, leach test, post-catalysis PXRD]. See DOI: 10.1039/x0xx00000x

In hopes of synthesizing a more dynamic system, we recently reported the incorporation of the Keggin-type POM, $[PW_{12}O_{40}]^{3-}$, into the microporous channels of the **csq**-net MOF, NU-1000 (PW_{12}@NU-1000, Figure 1).[42] In the report, the material was activated at 120 °C under vacuum prior to characterization, and the resulting material's crystallinity resembled that of the parent NU-1000.[43] Slight differences between the MOF and POM@MOF powder X-ray diffraction (PXRD) patterns were analyzed using difference envelope density (DED) analyses, which concluded that the electron density corresponding to the POM guest lied within the 12 Å microporous channels of NU-1000 and not the 31 Å mesoporous channels. The hierarchical framework allowed substrate diffusion and enhanced sulfide oxidation relative to the POM or MOF alone, while the interactions between the framework and POM were stable to leaching.

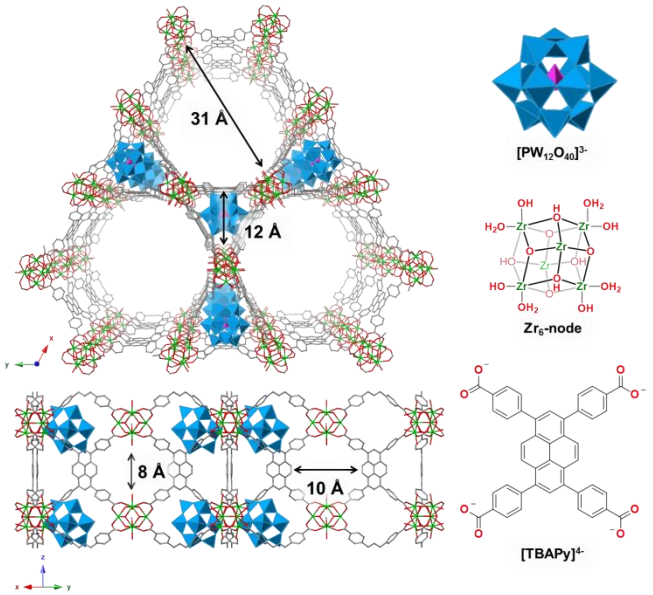

Figure 1. Structural representations (left) of the PW_{12}@NU-1000 previously published, also referred to as PW_{12}@NU-1000-120°C. Structures of the corresponding POM $[(PW_{12}O_{40})^{3-}]$, MOF node $[(Zr_6(\mu_3\text{-}O)_4(\mu_3\text{-}OH)_4(H_2O)_4(OH)_4)^{8+}]$, and MOF linker [1,3,6,8-tetrakis(p-benzoate)pyrene, $(TBAPy)^{4-}$] given (right). Light blue prisms=WO_5, pink prisms=PO_4, green=Zr, red=O, gray=C, hydrogen atoms omitted for clarity.

In the present work, we report the mild activation of PW_{12}@NU-1000 and the movement of the incorporated POM during heat exposure. The influence of the POM location on catalytic rate and selectivity of the composite are also investigated. To our knowledge, this is the first system where the location of POMs within a MOF can be monitored and controlled postsynthetically.

NU-1000 and PW_{12}@NU-1000-120°C were synthesized via previously published procedures.[42,44] PW_{12}@NU-1000-$scCO_2$ was prepared in a similar manner to PW_{12}@NU-1000-120°C, only differing in the method of solvent evacuation. Briefly, NU-1000 was soaked in an aqueous POM solution for three days. The composite was washed rigorously with water and anhydrous ethanol before activation by supercritical CO_2 drying (details in the Supporting Information).[45–47] PW_{12}@NU-1000-120°C can also be synthesized from PW_{12}@NU-1000-$scCO_2$ by heating the material in a 120 °C oven for at least one hour.

Both PW_{12}@NU-1000-$scCO_2$ and PW_{12}@NU-1000-120°C have a maximum loading of 0.8 POMs per Zr_6 node by inductively coupled plasma optical emission spectroscopy (ICP-OES) measurements of the acidic piranha-digested materials. Scanning electron microscopy (SEM) images indicate that the integrity and morphology of the crystallites are maintained during POM incorporation, and energy dispersive spectroscopy (EDS) line scans show a near uniform distribution of POM throughout the framework, except in the center of the crystal, where known defects occur (Figure S1).[43,48]

The powder X-ray diffraction (PXRD) pattern of PW_{12}@NU-1000-120°C resembles that of the parent NU-1000 (Figure 2). However, the PXRD pattern of PW_{12}@NU-1000-$scCO_2$ has peaks at similar d-spacing to PW_{12}@NU-1000-120°C, but very different intensities. Assuming no preferred orientation of MOF crystallites and retention of MOF structure, the peak intensities indicate major differences in guest location within the same unit cell. To understand the structural changes, in-situ variable temperature PXRD patterns were measured (Figure S2). The PW_{12}@NU-1000-$scCO_2$ sample was loaded into a rotating capillary and heated to and held at 120 °C. The evolution of the PW_{12}@NU-1000-$scCO_2$ sample pattern to the PW_{12}@NU-1000-120°C pattern was observed. This change was not reversible; the material retained the PW_{12}@NU-1000-120°C PXRD pattern upon cooling to room temperature.

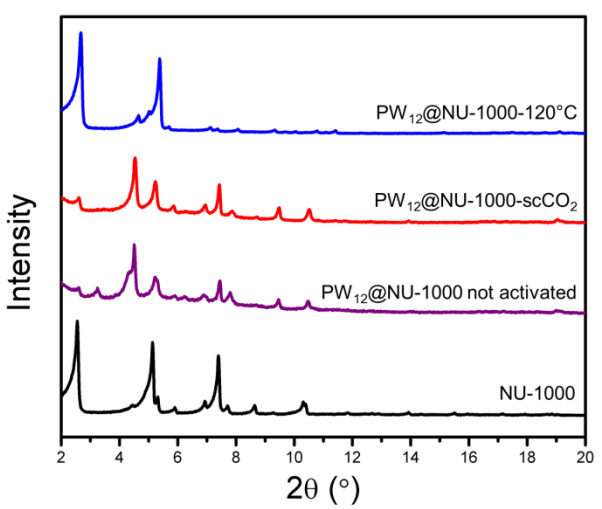

Figure 2. PXRD patterns for NU-1000 and PW_{12}@NU-1000 as-synthesized without solvent removal, activated by supercritical CO_2, and activated at 120 °C.

Inspired by the observed transformation in PXRD patterns, differential envelope density (DED) analyses were performed. DED analysis uses high intensity, low angle diffraction peaks generated by a synchrotron X-ray source to create an electron envelope. If the envelope of the parent material is known, its subtraction from the composite material results in a map of electron density corresponding to the guest molecules within a known structure.[49,50] By applying this technique to PW_{12}@NU-1000 composites, the electron density corresponding to the POMs were located close to the c-pore, the 8 × 10 Å windows in Figure 1 which connect the large and small channels, and in the hexagonal mesoporous channels of PW_{12}@NU-1000-scCO_2 (Figure 3 and S3), instead of residing in triangular microporous channels like in PW_{12}@NU-1000-120°C.[42] In both cases, the POMs resided on the same plane as the MOF nodes. Of note, the electron density in Figure S3 has six equally spaced areas around the mesopore corresponding to the POM guests' locations. The POMs likely are disordered over different orientations centered at these six sites. Additionally, if each of these sites were 100% occupied, then the expected POM loading would be 2 POMs/node. Because ICP-OES measurements calculated only a 0.8 POM/node loading, the electron clouds represent approximately 40% POM occupancy (idealized in Figure 3).

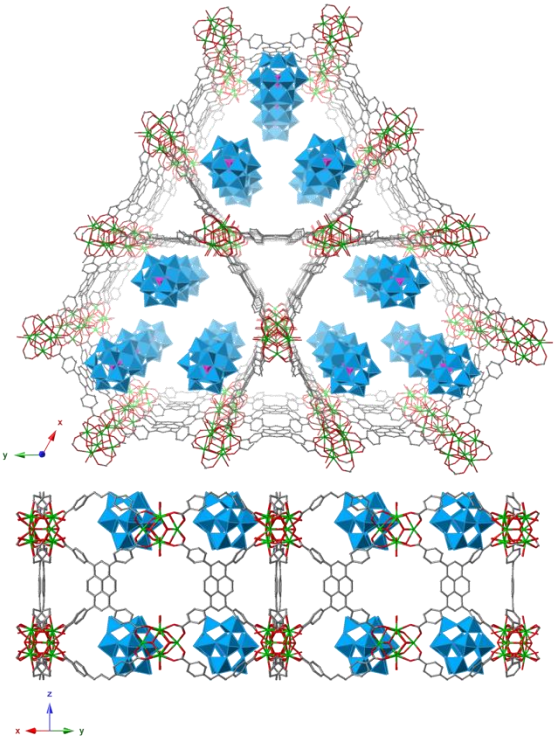

Figure 3. Structural representation of one possible POM conformation in PW_{12}@NU-1000-scCO_2 inferred by DED analysis. Light blue prism=WO_5, pink prism=PO_4, green=Zr, red=O, gray=C, hydrogen atoms omitted for clarity.

This location change manifests in other characterization techniques as well. Volumetric N_2 sorption isotherms and density functional theory (DFT) pore size distributions (Figure 4) reveal that PW_{12}@NU-1000-scCO_2 has a reduced mesopore volume, while PW_{12}@NU-1000-120°C has reduced micropore volume. These observations are in agreement with partial occupation of the mesopores or micropores in the respective samples. The Brunauer-Emmett-Teller (BET) areas of these materials are 1020, 850, and 700 m^3/cm^3 for NU-1000, PW_{12}@NU-1000-120°C, and PW_{12}@NU-1000-scCO_2. The differences in surface area between the two POM@MOF samples are attributed to the additional 5 wt% water present in the supercritical CO_2 activated sample, determined by TGA (Figure S4a). In the PW_{12}@NU-1000-scCO_2 sample, a small mass loss occurs around 170 °C, which has been observed with free $H_3PW_{12}O_{40}$, could be assigned to the loss of water that is hydrogen bonded to the acidic protons of the POM.[51] Around the same temperature in the TGA-DSC, a slight exothermic change in the heat flow rate of PW_{12}@NU-1000-scCO_2 could correlate to the POM movement from the mesopore to the micropore (Figure S4b). This exothermicity is consistent with POM positioned at an intrinsically favored binding site, possibly due to increased van der Waals interactions, as the POM is surrounded by only one pyrene linker in the mesopore and three pyrene linkers in the micropore. Interestingly, these interactions appear to be strong enough to immobilize the POM in the MOF, while also weak enough to allow POM movement.

Based on these observations, we believe the POMs sit in the mesopores close to the c-pore, when synthesized and remain there if no heat is applied (up to 80 °C). POM movement to the micropores is facilitated by elevated temperature coupled with partial removal of the POM's waters of hydration. Because of the consistent distribution of POM in the crystallite and its ability to change location in the absence of solvent, we propose that the POM migrates through the c-pore of NU-1000 to the more thermodynamically favorable micropore upon application of heat.

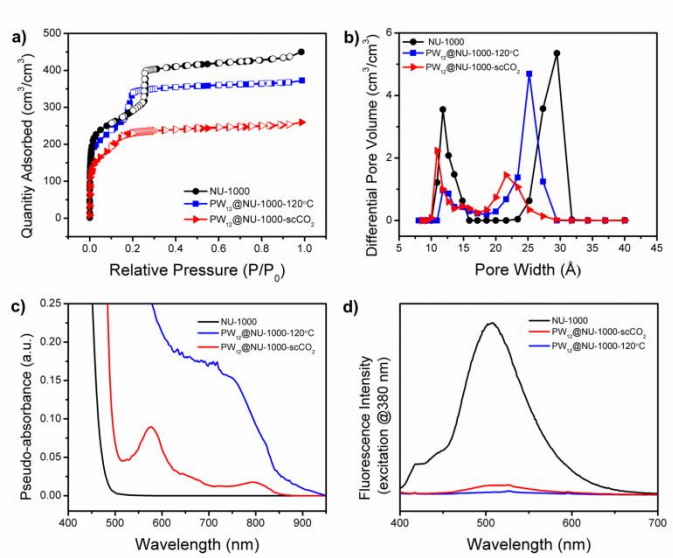

Figure 4. a) Volumetric N_2 isotherms collected at 77 K, b) DFT-calculated pore size distribution. c) Diffuse reflectance UV-vis

spectra, and d) emission spectra at 380 nm excitation of NU-1000, PW_{12}@NU-1000-$scCO_2$, and PW_{12}@NU-1000-120°C.

The different interactions of the POM and MOF as a function of location were also investigated spectroscopically. The ^{31}P MAS NMR spectrum of PW_{12}@NU-1000-$scCO_2$ is identical to free $H_3PW_{12}O_{40}$ (Figure S6). The ^{31}P signal shifts and become broader in PW_{12}@NU-1000-120°C, indicating loss of symmetry around the phosphorous and suggesting a strong interaction between the POM and the support.[52–54] In the cyclic voltammograms, the reduction events shift to more positive potentials from $H_3PW_{12}O_{40}$ to PW_{12}@NU-1000-120°C to PW_{12}@NU-1000-$scCO_2$ (Figure S7), again indicating stronger interaction of the POM with the pyrene in PW_{12}@NU-1000-$scCO_2$ since the composite is easier to reduce;[29,55] bare NU-1000 has no redox activity in the window scanned. Contrasting to the spectrum of bare NU-1000, a charge transfer band emerges in the diffuse reflectance UV-vis (DRUV-vis) spectra of both PW_{12}@NU-1000 samples (Figure 4c). In confirming the charge transfer mechanism, by fluorescence emission spectroscopy, PW_{12}@NU-1000-120°C and PW_{12}@NU-1000-$scCO_2$ quenched the pyrene's fluorescence 95% and 99%, respectively, after excitation at 380 nm (Figure 4d). These data suggest an efficient electron transfer from the excited pyrene-based linkers to the POM similar to what was observed when nickel bis(dicarbollide) was installed in NU-1000.[56] Of note, the evidence of interactions with the linker and the POM's position does not rule out potential interactions with the zirconia-like MOF nodes.[25,57]

With the knowledge that different activation procedures site the POM in either the mesopores or micropores and affect the electronic structure, we attempted to determine if the location impacted a substrate's accessibility to the catalytic sites. As a model reaction, we chose to study the oxidation of 2-chloroethyl ethyl sulfide (CEES) to 2-chloroethyl ethyl sulfoxide (CEESO) and 2-chloroethyl ethyl sulfone ($CEESO_2$) (Figure 5a). CEES is a simulant of the chemical warfare agent (CWA) mustard gas (HD or sulfur mustard), and one possible pathway for detoxification of HD involves oxidation of the central thioether to a sulfoxide.[58] However, over-oxidation to the sulfone yields another toxic compound.[59] Therefore, selectivity is paramount when designing materials for HD detoxification via oxidation.

Our previous findings[42] showed that in a 45 °C acetonitrile solution using H_2O_2 as an oxidant, NU-1000 nodes, with a structure similar to zirconia,[60,61] catalyzed the oxidation of CEES with a half-life (time to 50% conversion) of 13 min (Figure 5b) and preferred selectivity toward the doubly-oxidized product (Figure S8). Meanwhile under identical conditions, $H_3PW_{12}O_{40}$ was likewise active[62–64] with a half-life of 5 min and preferred selectivity for the singly-oxidized product. The composite PW_{12}@NU-1000-120°C, normalized to the total number of active clusters (POMs and MOF nodes), decreased the half-life of the reaction to 3 min with an intermediate selectivity of 59 ± 7%. PW_{12}@NU-1000-$scCO_2$ further reduces the half-life of CEES conversion to 1 min with a greater selectivity (90 ± 5%) for the preferred singly oxidized product. Because the initial rate of reaction using 2 mol% catalyst was too fast for time points with low conversion to be collected reliably, initial turnover frequencies (TOFs) were therefore determined using 1 mol% catalyst (Figure S9). The TOF of PW_{12}@NU-1000-$scCO_2$ was found to be about 3 times higher than that of PW_{12}@NU-1000-120°C.

The difference in selectivity has been attributed to the different mechanisms which occur on the MOF node or the POM.[60,65,66] The intermediate selectivity when using PW_{12}@NU-1000-120°C could indicate that both the POM and MOF are accessible. The micropores are blocked so access to the POM requires diffusion through the windows connecting the channels, which has been observed and calculated in other NU-1000-based systems.[67,68] When the POMs are situated in the mesopores, diffusion of the substrate to POM is no longer hindered; and therefore, the sulfide readily reacts with the POM to produce the singly-oxidized product almost exclusively. Since these reactions are normalized to the number of active clusters, the increased activities of the composites compared to the individual components alone are attributed to the stabilization of in the POM on the MOF. Leach tests confirm these reactions occur heterogeneously (Figure S9) and post-catalysis PXRD patterns indicate the POMs do not move during catalysis (Figure S10).

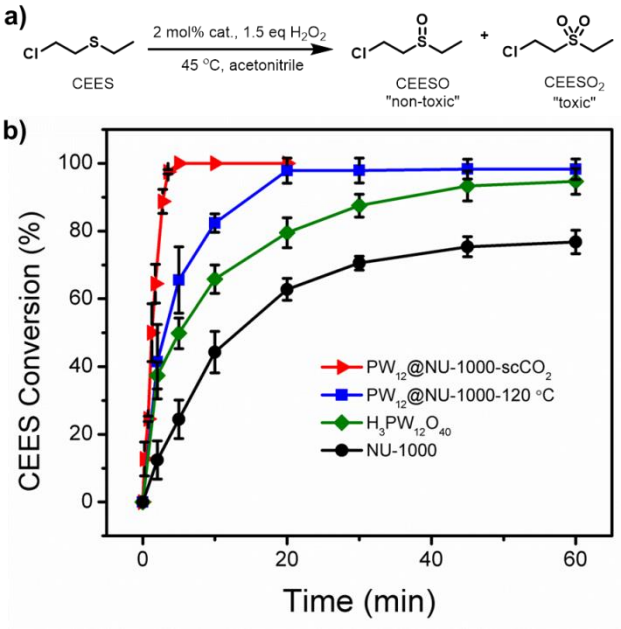

Figure 5. a) Scheme of the reaction pathway for the oxidation of CEES to CEESO and $CEESO_2$ under the conditions presented in this work. b) Reaction profiles for the reaction in a) using the catalysts: NU-1000, $H_3PW_{12}O_{40}$, PW_{12}@NU-1000-120°C, and PW_{12}@NU-1000-$scCO_2$.

Conclusions

PW_{12}@NU-1000 has been synthesized by postsynthetic incorporation of $[PW_{12}O_{40}]^{3-}$ in NU-1000. The composite material was activated by using supercritical CO_2 and by 120 °C under vacuum. Differences in the diffraction patterns of these materials suggested that the POMs are located in the mesopores when supercritical CO_2 is used to evacuate the pores of solvent molecules and migrate to the micropores when heated to 120 °C; these structural changes were corroborated by sorption and spectroscopic properties. PW_{12}@NU-1000-scCO_2 displayed a faster rate of reaction and higher product selectivity in the partial oxidation of CEES, a mustard gas simulant. To our knowledge, this is the first system where a POM catalyst can be monitored and controlled postsynthetically within a MOF. These findings highlight the importance of knowing and controlling catalyst location to engender favorable synergistic effects between a catalyst and support. Current efforts aim to identify other systems with similar control over catalyst location.

Conflicts of interest

There are no conflicts to declare.

Acknowledgements

O.K.F. gratefully acknowledges support from the Defense Threat Reduction Agency (HDTRA1-18-1-0003). C.T.B. acknowledges Joseph T. Hupp for his helpful discussions. Metal analysis was performed at the Northwestern University Quantitative Bio-element Imaging Center. D.G.C. was supported by NSF grant DMR-1708254. This work made use of the EPIC facility of Northwestern University's NUANCE Center, which has received support from the Soft and Hybrid Nanotechnology Experimental (SHyNE) Resource (NSF NNCI-1542205); the MRSEC program (NSF DMR-1121262) at the Materials Research Center; the International Institute for Nanotechnology (IIN); the Keck Foundation; and the State of Illinois, through the IIN. This work made use of the IMSERC at Northwestern University, which has received support from the NSF (CHE-1048773 and DMR-0521267); Soft and Hybrid Nanotechnology Experimental (SHyNE) Resource (NSF NNCI-1542205); the State of Illinois and International Institute for Nanotechnology (IIN). Work done at Argonne was performed using the Advanced Photon Source, a U.S. Department of Energy (DOE) Office of Science User Facility operated for the DOE Office of Science by Argonne National Laboratory under Contract No. DE-AC02-06CH11357.

Notes and references

(1) Yang, X.-F.; Wang, A.; Qiao, B.; Li, J.; Liu, J.; Zhang, T. *Acc. Chem. Res.* **2013**, *46* (8), 1740–1748.

(2) Yang, D.; Odoh, S. O.; Wang, T. C.; Farha, O. K.; Hupp, J. T.; Cramer, C. J.; Gagliardi, L.; Gates, B. C. *J. Am. Chem. Soc.* **2015**, *137*, 7391–7396.

(3) Byun, J.; Patel, H. A.; Kim, D. J.; Jung, C. H.; Park, J. Y.; Choi, J. W.; Yavuz, C. T. *J. Mater. Chem. A* **2015**, *3*, 15489–15497.

(4) Collman, J. P.; Hegedus, L. S.; Cooke, M. P.; Norton, J. R.; Dolcetti, G.; Marquardt, D. N. *J. Am. Chem. Soc.* **1972**, *94* (5), 1789–1790.

(5) Michalska, B. Z. M.; Webster, D. E. *Platin. Met. Rev.* **1974**, *18* (2), 65–73.

(6) Mines, P. D.; Byun, J.; Hwang, Y.; Patel, H. A.; Andersen, H. R.; Yavuz, C. T. *J. Mater. Chem. A* **2015**, *4*, 632–639.

(7) Mcmorn, P.; Hutchings, G. J. *Chem. Soc. Rev.* **2004**, *33*, 108–122.

(8) Wegener, S. L.; Marks, T. J.; Stair, P. C. *Acc. Chem. Res.* **2012**, *45* (2), 206–214.

(9) Munnik, P.; de Jongh, P. E.; de Jong, K. P. *Chem. Rev.* **2015**, *115*, 6687–6718.

(10) Védrine, J. C. *Appl. Catal. A, Gen.* **2014**, *474*, 40–50.

(11) Zhang, D.; Li, X.; Liu, S.; Zhu, X.; Chen, F.; Xu, L. *Chem. - An Asian J.* **2015**, *10* (8), 1647–1659.

(12) Mejía, C. H.; Otter, J. H. Den; Weber, J. L.; Jong, K. P. De. *Appl. Catal. A, Gen.* **2017**, *548*, 143–149.

(13) Bligaard, T.; Nørskov, J. K. *Chem. Bond. Surfaces Interfaces* **2008**, *98* (96), 255–321.

(14) Hill, C. L.; Kholdeeva, O. A. In *Liquid Phase Oxidation via Heterogeneous Catalysis: Organic Synthesis and Industrial Applications*; Clerici, M. G., Kholdeeva, O. A., Eds.; John Wiley & Sons, Inc.: Hoboken, NJ, 2013; pp 263–319.

(15) Ye, J.; Wu, C. *Dalt. Trans.* **2016**, *45*, 10101–10112.

(16) Pope, M. *Heteropoly and Isopoly Oxometalates*; Springer-Verlag: New York, 1983.

(17) Gouzerh, P.; Proust, A. *Chem. Rev.* **1998**, *98* (1), 77–112.

(18) Hill, C. L. *Compr. Coord. Chem. II* **2004**, *4*, 679–759.

(19) Long, D.-L.; Burkholder, E.; Cronin, L. *Chem. Soc. Rev.* **2007**, *36* (1), 105–121.

(20) Kozhevnikov, I. V. *Chem. Rev.* **1998**, *98* (1), 171–198.

(21) Izumi, Y.; Urabe, K. *Chem. Lett.* **1981**, *10* (5), 663–666.

(22) Genovese, M.; Lian, K. *J. Mater. Chem. A* **2017**, *5*, 3939–3947.

(23) Fazaeli, R.; Aliyan, H.; Ahmadi, M. A.; Hashemian, S. *Catal. Commun.* **2012**, *29*, 48–52.

(24) Thompson, D. J.; Zhang, Y.; Ren, T. *J. Mol. Catal. A Chem.* **2014**, *392*, 188–193.

(25) Herna, J. G.; Corte, M. A.; Lo, E.; Armenda, H.; Lo, T. *Appl. Catal. A, Gen.* **1998**, *175*, 43–53.

(26) Lauinger, S. M.; Sumliner, J. M.; Yin, Q.; Xu, Z.; Liang, G.; Glass, E. N.; Lian, T.; Hill, C. L. **2015**.

(27) Gao, W.; Sun, X.; Niu, H.; Song, X.; Li, K.; Gao, H. *Microporous Mesoporous Mater.* **2015**, *213*, 59–67.

(28) Lefebvre, F. *Inorganics* **2016**, *4* (2), 13.

(29) Salomon, W.; Roch-Marchal, C.; Mialane, P.; Rouschmeyer, P.; Serre, C.; Haouas, M.; Taulelle, F.; Yang, S.; Ruhlmann, L.; Dolbecq, A. *Chem. Commun.* **2015**, *51* (14), 2972–2975.

(30) Gomez-mingot, M.; Roch-marchal, C.; Lassalle-kaiser, B.; Mialane, P.; Fontecave, M.; Mellot-draznieks, C.; Dolbecq, A. *J. Am. Chem. Soc.* **2017**, DOI: 10.1021/jacs.7b11788.

(31) Zhou, H. C.; Long, J. R.; Yaghi, O. M. *Chem. Rev.* **2012**, *112* (2), 673–674.

(32) Howarth, A. J.; Peters, A. W.; Vermeulen, N. A.; Wang, T. C.; Hupp, J. T.; Farha, O. K. *Chem. Mater.* **2016**, 26–39.

(33) Howarth, A. J.; Liu, Y.; Li, P.; Li, Z.; Wang, T. C.; Hupp, J. T.; Farha, O. K. *Nat. Rev. Mater.* **2016**, *1*, No. 15018.
(34) Juan-Alcañiz, J.; Gascon, J.; Kapteijn, F. *J. Mater. Chem.* **2012**, *22*, 10102–10118.
(35) Du, D.-Y.; Qin, J.-S.; Li, S.-L.; Su, Z.-M.; Lan, Y.-Q. *Chem. Soc. Rev.* **2014**, *43* (13), 4615–4632.
(36) Chen, L.; Luque, R.; Li, Y. *Chem. Soc. Rev.* **2017**, *46*, 4614–4630.
(37) Bromberg, L.; Su, X.; Hatton, T. A. *ACS Appl. Mater. Interfaces* **2013**, *5*, 5468–5477.
(38) Salomon, W.; Yazigi, F.-J.; Roch-Marchal, C.; Mialane, P.; Horcajada, P.; Serre, C.; Haouas, M.; Taulelle, F.; Dolbecq, A. *Dalt. Trans.* **2014**, *43* (33), 12698–12705.
(39) Férey, G.; Mellot-Draznieks, C.; Serre, C.; Millange, F.; Dutour, J.; Surblé, S.; Margiolaki, I. *Science* **2005**, *309* (5743), 2040–2042.
(40) Bromberg, L.; Diao, Y.; Wu, H.; Speakman, S. A.; Hatton, T. A. *Chem. Mater.* **2012**, *24* (9), 1664–1675.
(41) Bromberg, L.; Hatton, T. A. *ACS Appl. Mater. Interfaces* **2011**, *3*, 4756–4764.
(42) Buru, C. T.; Li, P.; Mehdi, B. L.; Dohnalkova, A.; Platero-Prats, A. E.; Browning, N. D.; Chapman, K. W.; Hupp, J. T.; Farha, O. K. *Chem. Mater.* **2017**, *29* (12), 5174–5181.
(43) Mondloch, J. E.; Bury, W.; Fairen-Jimenez, D.; Kwon, S.; Demarco, E. J.; Weston, M. H.; Sarjeant, A. A.; Nguyen, S. T.; Stair, P. C.; Snurr, R. Q.; Farha, O. K.; Hupp, J. T. *J. Am. Chem. Soc.* **2013**, *135* (28), 10294–10297.
(44) Wang, T. C.; Vermeulen, N. A.; Kim, I. S.; Martinson, A. B. F.; Stoddart, J. F.; Hupp, J. T.; Farha, O. K. *Nat. Protoc.* **2015**, *11* (1), 149–162.
(45) Nelson, A. P.; Farha, O. K.; Mulfort, K. L.; Hupp, J. T. *J. Am. Chem. Soc.* **2009**, *131*, 458–460.
(46) Farha, O. K.; Shultz, A. M.; Sarjeant, A. A.; Nguyen, S. T.; Hupp, J. T. *J. Am. Chem. Soc.* **2011**, *133*, 5652–5655.
(47) Shultz, A. M.; Farha, O. K.; Adhikari, D.; Sarjeant, A. A.; Hupp, J. T.; Nguyen, S. T. *Inorg. Chem.* **2011**, *50*, 3174–3176.
(48) Webber, T. E.; Liu, W.; Desai, S. P.; Lu, C. C.; Truhlar, D. G.; Penn, R. L. *ACS Appl. Mater. Interfaces* **2017**, *9*, 39342–39346.
(49) Yakovenko, A. A.; Wei, Z.; Wriedt, M.; Li, J.-R.; Halder, G. J.; Zhou, H. *Cryst. Growth Des.* **2014**, *14*, 5397–5407.
(50) Gallington, L. C.; Kim, I. S.; Liu, W. G.; Yakovenko, A. A.; Platero-Prats, A. E.; Li, Z.; Wang, T. C.; Hupp, J. T.; Farha, O. K.; Truhlar, D. G.; Martinson, A. B. F.; Chapman, K. W. *J. Am. Chem. Soc.* **2016**, *138* (41), 13513–13516.
(51) Fournier, M.; Feumi-Jantou, C.; Rabia, C.; Herve, G.; Launay, S. *J. Mater. Chem.* **1992**, *2* (9), 971–978.
(52) Lefebvre, F. *J. Chem. Soc., Chem. Commun.* **1992**, *0*, 756–757.
(53) Damyanova, S.; Fierro, J. L. G.; Sobrados, I.; Sanz, J. *Langmuir* **1999**, *15* (2), 469–476.
(54) Sofia, L. T. A.; Krishnan, A.; Sankar, M.; Raj, N. K. K.; Manikandan, P.; Rajamohanan, P. R.; Ajithkumar, T. G. *J. Phys. Chem. C* **2009**, *113*, 21114–21122.
(55) De Sousa, P. M. P.; Grazina, R.; Barbosa, A. D. S.; De Castro, B.; Moura, J. J. G.; Cunha-Silva, L.; Balula, S. S. *Electrochim. Acta* **2013**, *87*, 853–859.
(56) Kung, C.; Otake, K.; Buru, C. T.; Goswami, S.; Cui, Y.; Hupp, J. T.; Spokoyny, A. M.; Farha, O. K. *J. Am. Chem. Soc.* **2018**, DOI: 10.1021/jacs.8b00605.
(57) López-salinas, E.; Hernández-cortéz, J. G.; Schifter, I.; Torres-Garcia, E.; Navarrete, J.; Gutierrez-Carrillo, A.; Lopez, T.; Lottici, P. P.; Bersani, D. *Appl. Catal. A, Gen.* **2000**, *193*, 215–225.
(58) Riches, J.; Read, R. W.; Black, R. M. *J. Chromatogr. B Anal. Technol. Biomed. Life Sci.* **2007**, *845* (1), 114–120.
(59) Hirade, J.; Ninomiya, A. *J. Biochem.* **1950**, *37*, 19–34.
(60) Lousada, C. M.; Johansson, A. J.; Brinck, T.; Jonsson, M. *J. Phys. Chem. C* **2012**, *116* (17), 9533–9543.
(61) Faccioli, F.; Bauer, M.; Pedron, D.; Sorarù, A.; Carraro, M.; Gross, S. *Eur. J. Inorg. Chem.* **2015**, *2015* (2), 210–225.
(62) Fazaeli, R.; Aliyan, H.; Masoudinia, M.; Heidari, Z. *J. Mater. Chem. Eng.* **2014**, *2* (2), 46–55.
(63) Ebrahimi, N.; Fazaeli, R.; Aliyan, H. *Zeitschrift fuer Naturforsch. B* **2016**, *71* (3), 211–217.
(64) Frenzel, R.; Pizzio, L.; Blanco, M.; Sathicq, G.; Romanelli, G. *Curr. Catal.* **2016**, *5* (3), 124–130.
(65) Frenzel, R.; Morales, D.; Romanelli, G.; Sathicq, G.; Blanco, M.; Pizzio, L. *J. Mol. Catal. A Chem.* **2016**, *420*, 124–133.
(66) Doherty, S.; Knight, J. G.; Carroll, M. A.; Clemmet, A. R.; Ellison, J. R.; Backhouse, T.; Holmes, N.; Thompson, L. A.; Bourne, R. A. *RSC Adv.* **2016**, *6*, 73118–73131.
(67) Vargas L., E.; Snurr, R. Q. *Langmuir* **2015**, *31*, 10056–10065.
(68) Li, P.; Modica, J. A.; Howarth, A. J.; Vargas L., E.; Moghadam, P. Z.; Snurr, R. Q.; Mrksich, M.; Hupp, J. T.; Farha, O. K. *Chem* **2016**, *1* (1), 154–169.

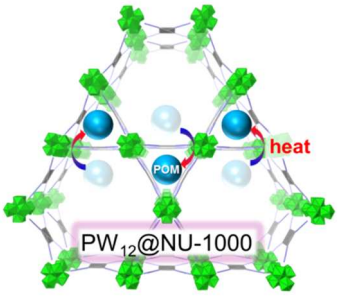

A polyoxometalate supported by the metal–organic framework, NU-1000, undergoes migration from the mesopore to the micropore when heated.